AIAA JOURNAL
Vol. 35, No. 10, October 1997

Instantaneous Three-Dimensional Vorticity Measurements in Vortical Flow over a Delta Wing

A. Honkan* and J. Andreopoulos†
City College of the City University of New York, New York, New York 10031

An attempt is made to explore the structures in the vortical flow over a delta wing by spatio–temporal measurements of velocity vectors and subsequent evaluation of vorticity vectors. A novel probe, with good spatial resolution, to measure the multipoint velocity vector has been designed and constructed. Tests results of the statistical properties from the measurements of instantaneous velocity and vorticity vectors in the turbulent boundary layers gave confidence to investigate the vortices over a 45-deg-swept-back delta wing and to explore their complex structure with this probe. The present measurements indicated the existence of discrete stationary vortices in the feeding shear layer region as well as a primary vortex where mean vorticity is at maximum and where the mean velocity excess is about $1.3U_0$. Large vorticity fluctuations, of the order of three to six times the mean vorticity, were measured between the low speed side of the shear layer and the surface of the delta wing. Such fluctuating vorticity statistics are presented for the first time. The shear layer reattachment zone and the region of secondary separation are associated with intense turbulence activities. It is also shown for the first time that secondary vorticity of alternating sign is generated at the wall of the delta wing through measurements of time- and space-resolved wall vorticity flux.

Nomenclature

c_{pI}	= rms of pressure fluctuations coefficient $p\prime/(1/2\rho U_0^2)$
Re	= Reynolds number based on chord length
S_{ik}	= rate of strain tensor
s	= semispan
U, V, W	= instantaneous velocity components along x, y, and z directions, respectively
U_0	= freestream velocity
u, v, w	= velocity fluctuations about mean along x, y, and z directions
α	= angle of attack
Γ	= circulation
ε	= dissipation rate of turbulent kinetic energy
η	= Kolmogorov length scale, $[\nu^3/\varepsilon]^{1/4}$
θ	= $\tan^{-1}\Delta\omega_x/\Delta\omega_z$ orientation angle of σ_w
Λ	= swept-back angle
μ	= fluid viscosity
ν	= kinematic viscosity
ρ	= fluid density
σ	= vorticity flux vector, $(\partial\omega_x/\partial y, \partial\omega_y/\partial y, \partial\omega_z/\partial y)$
σ_w	= vorticity flux tangential to the wall, $(\partial\omega_x/\partial y, \partial\omega_z/\partial y)$
$\Omega_x, \Omega_y, \Omega_z$	= instantaneous vorticity components along x, y, and z directions, respectively
ω	= vorticity fluctuation
$\omega_x, \omega_y, \omega_z$	= vorticity fluctuations about mean along x, y, and z directions, respectively
$\frac{1}{2}q^2$	= turbulent kinetic energy, $\frac{1}{2}(\overline{u^2}+\overline{v^2}+\overline{w^2})$
$\frac{1}{2}\omega_i\omega_i$	= enstrophy, $\frac{1}{2}[\overline{\omega_x^2}+\overline{\omega_y^2}+\overline{\omega_z^2}]$

I. Introduction

THE role of vorticity in gaining further insight into the origin, evolution, and structure of vortex-dominated aerodynamic flows is well established. However, progress in better understanding several of the physical aspects of these flows is hampered by the lack of experimental techniques capable of measuring accurately three-dimensional, time-dependent vorticity. The most typical example of vortex-dominated flows, which is of great importance due to its significance in applications, is the flow over a delta wing.

When a flow approaches a delta wing pitched at certain angle of attack, two spiraling vortices are formed as the flow separates into a pair of shear layers at the leading edges.[1,2] These vortices increase in size as they are convected downstream by the streamwise velocity of the outer flow. It has been shown by many investigators that strong vortices in proximity to a solid surface can induce an adverse pressure gradient at the wall, which can cause unsteady separation of the wall layer and promote the generation of opposite vorticity,[3,4] which enters the flow from the upper wall in the form of the so-called secondary vortex.

The development of highly maneuverable airplanes has prompted a significant amount of research that is focused mainly on the dynamic stall and vortex breakdown phenomena associated with the sudden pitching motions of airfoils.[5–9] Ironically, the structure and the behavior of the vortical flow over a stationary delta wing has attracted less attention although an appreciable amount of the lift is generated by this pair of vortices. Because of the enhanced lift, stalling of the delta wing is delayed for larger angles of attack that are beyond stall for conventional wing forms.

In the literature there appear to be many flow visualization experiments carried out in air or water,[10–14] a few with mean velocity measurements,[11,14,15] several investigations with one component of mean vorticity measurement,[16,17,19,35] one with very limited turbulence measurements,[11] and many computational studies of the flow over delta wing with unburst vortices.[18,29]

The feeding shear layer emanating from the leading edge has been observed in flow visualizations by Gad-el-Hak and Blackwelder[11] to roll periodically into discrete vortical structures, which grow by pairing. Vortical substructures, which rotate around the primary vortex, are formed. The formation of these vortices is attributed to Kelvin–Helmholz instability. Smoke flow visualizations by Payne et al.[14] in highly swept delta wings indicated the formation of stationary cellular substructures that do not rotate around the primary vortex. Lowson et al.[16] also observed similar structures in the same delta wing geometries and Reynolds numbers, which, however, disappeared at higher Reynolds numbers. Washburn and Visser[19] attributed the presence of ordered vortical structures to crossflow instabilities.

Flow visualization experiments maybe very misleading because the diffusion coefficient of dye or smoke is considerably higher than the diffusion coefficient of vorticity. The transport equation of vorticity is

$$\frac{D\Omega_i}{Dt} = S_{ik}\Omega_k + \nu\frac{\partial^2\Omega_i}{\partial x_k \partial x_k} \tag{1}$$

Received May 18, 1995; revision received May 19, 1997; accepted for publication June 16, 1997.

*Graduate Research Assistant, Experimental Fluid Mechanics and Aerodynamics Laboratory, Department of Mechanical Engineering. Member AIAA.

†Professor, Experimental Fluid Mechanics and Aerodynamics Laboratory, Department of Mechanical Engineering. Associate Fellow AIAA.

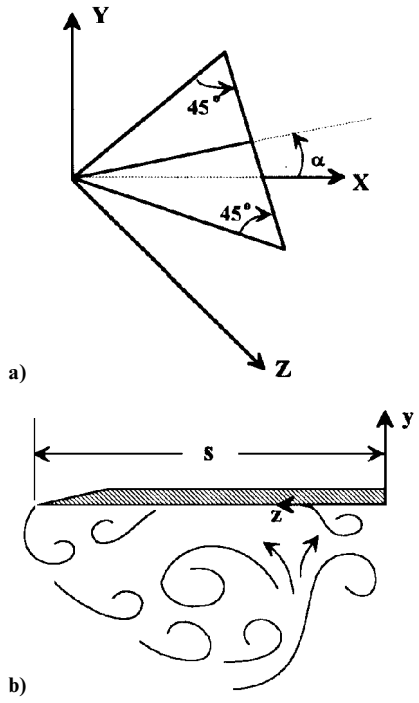

Fig. 1 Coordinate system and flow structure.

and it is obvious that the diffusion coefficient is the fluid viscosity ν and, therefore, the Schmidt number of the dye used may be greater than 1. Thus, the vorticity/momentum interface may be different from the dye interface. Quantitative measurement of vorticity appears to be the best way to explore the highly ordered structures of the shear layer, which are of great fundamental interest.

The present experiment attempts to address the role of vorticity distribution in the leading-edge vortices over a delta wing of 45-deg-sweep angle for the first time. This particular geometry for the model was chosen for two reasons: 1) extrapolation of existing data allowed to safely assume no vortex breakdown,[11] and 2) no time-dependent velocity/vorticity vector measurements were attempted for such low-sweep triangular planforms. In addition, the structure of the near wall flow close to the reattachment and secondary separation is investigated by means of some novel measurements of wall vorticity flux. This term is very important in understanding vorticity dynamics in a particular flow because it represents the rate of creation of vorticity at a solid boundary, which subsequently is shed inside the flow.

The major feature of the present contribution is the high-resolution measurement of turbulence, in space as well as in time. The spatial resolution of our vorticity probe is of the order of four Kolmogorov viscous microscales. To the best of our knowledge, these data represent the most resolved measurements of vorticity in a flow over a delta wing. Our vorticity flux data are equally well resolved in space and time.

The results obtained can provide guidance in turbulence modeling, improve calculation methods for vortical flows, and help in better understanding some of the physics of the flow.

Experimental Setup

Flow Facility

All of the experimental investigations were carried out in the wind tunnel of Mechanical Engineering Department, City College of the City University of New York. It is an open-ended suction type with a 4×4 ft cross section and a 20-ft-long working area. To minimize vibrations, the working section was isolated from the downstream fan and motor.

The 45-deg-sweep delta wing model was fabricated from 9.5-mm aluminum stock and has a root chord of 305 mm and span of 610 mm, thus giving an aspect ratio of 4:1. The leading edges were beveled at 30 deg, whereas the trailing edge was square. The model is suspended in the center of the working section of the wind tunnel with the help of a supporting mechanism, which consisted of two aluminum struts hinged on the bracket fitted on the top of the wind tunnel. A cross member across the two struts made the model stay rigid in the flow and also allowed for a lead screw to be mounted inside in such a way as to enable the wing to be pitched at any desired angle of attack between 0 and 45 deg. The model was installed inverted in the tunnel, as shown in Fig. 1a. Figure 1b is a sketch of the expected flow structure associated with the inverted position of the model.

Instrumentation

A better understanding of the vortical structure of the flow requires measurements of highly fluctuating velocity vectors. A careful use of triple orthogonal hot-wire probes (TOW) can provide the required information in this three-dimensional separated flow, which contains rather limited reverse flow regions. Such probes have been used extensively in the past, and the techniques associated with their application have been described by Andreopoulos[20] and Andreopoulos and Honkan.[34,36] Error analysis[21] has shown that the expected uncertainties range from 6% in the regions of 30% turbulence intensity to 12% in the regions with 50% turbulence intensity. Measurements in flows with turbulence intensities higher than 50% should be interpreted with caution, and the methodology suggested by Maciejewski and Moffat[22] should be adopted. The vorticity probe consisted of three triple hot-wire probes.

The hot-wire sensors of the vorticity probe were operated by nine-channel constant temperature anemometers, model 56CO1/C17 manufactured by Dantec Electronics, Inc.

Pressure fluctuations were measured by high-frequency response and high-sensitivity, subminiature, Kulite® pressure transducers model XCS-62-5-D. For the measurements of wall pressure gradients in two directions and, therefore, the evaluation of vorticity flux away from the wall, four of these transducers were used.[4] The module with the four transducers was inserted in two different positions on the delta wing, one on the line of symmetry at $z/s = 0.0$ and a second at $z/s = 0.5$, both at $X/c = 0.7$. The location off the centerline is approximately below the primary vortex.

In situ calibrations, including those for yaw and pitch response of the probe, were carried out in the inviscid core of the flow, once prior to the data acquisition session and then at the end of the experiment. Details of the techniques and estimates of scales resolution by the probe are provided by Refs. 23–25 and 34.

The 3TOW probe was placed in the delta wing flow with freestream velocity of 3 m/s and Reynolds number based on the chord of the delta wing $Re = 5.8615 \times 10^4$. The anemometer outputs of all nine hot-wires were low-pass filtered at 2 kHz and were observed on the oscilloscopes before digitizing at a 5-kHz sampling rate. The data were collected for about 61 s and streamed to the hard drive before mass storage on tapes. The flowfield was scanned at several spanwise and normal positions at 15-deg angle of attack. At each measurement location, the probe axis was aligned appropriately with the anticipated mean flow direction while the ambient temperature was monitored at regular intervals.

The problem of spatial resolution of the probe is the most important issue in the measurements of vorticity fluctuations. It has been shown[26,28] that most of the contributions to vorticity fluctuations come from the high wave number of the spectrum, i.e., small scales that are of the order of the Kolmogorov length scale η. If the probe size is very large in comparison to η, then spatial attenuation will result in considerably underestimated statistics of vorticity fluctuations. Estimates of the flow scales in the present case indicated that the resolution of each of the individual 3TOW probes was of the order of 2η, whereas the separation among them was about 4η. Thus, the present highly resolved measurements of vorticity can provide information down to the dissipative scales of turbulence.

A wet surface technique was used to identify the flow structure at the wall of the wing. Carbon powder was mixed with small quantities of deodorized kerosene, and the mixture was spread on the entire surface of the delta wing.

The vortical structures of the flow above the delta wing were visualized by using smoke illuminated by a thin light sheet from an Ar^+ laser. The sheet was formed by the reflection of the laser beam on rotating mirrors. The smoke was introduced at the apex

of the wing through internal tubing or upstream of the wing by a small-diameter brass tube. The visual observations were recorded by a charge-coupled-devicevideo camera. All images were postprocessed by using a frame grabber and appropriate image processing software.

Results

To assess the performance of the vorticity probe, measurements of the velocity and vorticity fields in the zero pressure gradient boundary layer were carried out first. The results of this investigation were compared with the experimental data of Balint et al.[26] and the direct numerical simulation results of Spalart.[27] Details of this comparison are described by Honkan[23] and Honkan and Andreopoulos[28] and in the recent review article by Wallace and Foss.[31]

Note that, whereas the resolution in the boundary layer experiment was of the order of eight Kolmogorov viscous scales, the resolution in the present experiment has been improved to four Kolmogorov scales.

The viscous sublayer of the turbulent boundary layer contains higher mean velocity gradients and/or vorticity than the delta wing vortices. At $y^+ = 12.5$, the location closest to the wall where measurements were obtained, the mean velocity gradient is about $dU^+/dy^+ = 0.35$, which corresponds to $dU/dy \approx 380\ s^{-1}$. This value is very close to theoretical predictions. In the delta wing experiment, the maximum nondimensional vorticity (shown in a subsequent figure) is about 25, which corresponds to about 250 s^{-1}. Thus, the viscous sublayer was a more severe test for the probe than that of the delta wing vortex.

What is important, however, is not the mean velocity gradient but its instantaneous value, which includes the fluctuating part. Thus, the probe should be able to respond to the demands of the instantaneous vorticity vector. The reason is that in both flows vorticity fluctuations are large, i.e., of the order of the mean vorticity or higher. The rms of the fluctuations is about 270 s^{-1} in the boundary layer and about 300 s^{-1} in the delta wing. Thus, the magnitude of the instantaneous vorticity is about the same. In fact, both experiments were designed to provide similar flow conditions and to maximize spatial resolution.

It also appears that the agreement of the boundary-layer data with the data of Balint et al.[26] is very satisfactory. This provides confidence in the experimental techniques used in the present investigation.

The flow visualization studies indicated the absence of vortex breakdown over the delta wing. A leading vortex with an isolated center was observed, and a smaller secondary vortex close to the surface was also visible. Secondary vortical structures in the feeding shear layer have been identified in many flow images. Figure 2 shows the primary vortex in a lateral cross section at 15-deg angle of attack obtained at a cross section of $X/c = 0.85$. Figures 3 and 4 show imprints of the limiting streamlines on the surface of the delta wing at $\alpha = 20$ and 40 deg, respectively. The direction of the oil streaks represents the direction of the wall mean shear, whereas an indication of the shear stress magnitude can be obtained from the amount of oil (white color) deposited on the streaks, this being greater at low shear areas. Thus, dark regions are characterized by high shear and may be associated with flow reattachment, whereas light regions indicate low shear regions, which are closely related to separation. Accordingly, the reattachment line at $X/c = 0.85$ is located at about $z/s = 0.25$, and the secondary separation line at about $z/s = 0.66$ in the case of $\alpha = 20$ deg. As the angle of attack increases, both lines move toward the plane of symmetry and the two primary vortices start to approach each other while at the same time they keep inducing the common fluid between them to move toward the wing surface. At $\alpha = 40$ deg, both shear layers are in contact and directly interact with each other. As a result of the induced flow reattachment on the wing surface and the interaction of the two shear layers, the pressure field at the surface is highly fluctuating. This is shown in Fig. 5, where the rms of pressure fluctuations measured at the plane of symmetry at $X/c = 0.7$ is plotted vs the angle of attack. At small values of α, the level of fluctuations is small. For $\alpha > 15$ deg, the rms suddenly increases and peaks at $\alpha = 20$ deg with a value 3.5 times larger than that at $\alpha = 0$ deg. When the angle of attack further increases, the rms drops to a smaller value, which remains constant for all $\alpha > 25$ deg. In unseparated two-dimensional turbulent boundary layers, the rms of wall pressure fluctuations is related to the local skin-friction coefficient. However, in the present case the high level of pressure fluctuations at the plane of symmetry $z/s = 0$ is associated with fluid impinging on the wing surface. The helical motion of the fluid induced by the primary vortex causes the flow to reattach, resulting in high-pressure fluctuations, which appear to be correlated with the normal-to-the-surface velocity component V rather than with the U or W. At $\alpha = 20$ deg, it appears that the outer part of the shear layer is impinging the surface at the line of symmetry, resulting in an increase in the amplitude of pressure fluctuations.

The level of pressure fluctuations at $z/s = 0.5$ as a function of the angle of attack is also shown in Fig. 5. Large pressure fluctuations have been measured at small angles of attack, which is indicative of flow impingement at this location. As α increases, the level of

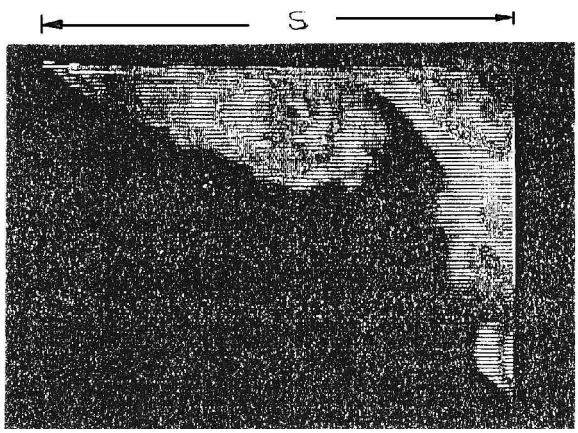

Fig. 2 Photograph of flow by a laser sheet at $X/c = 0.85$.

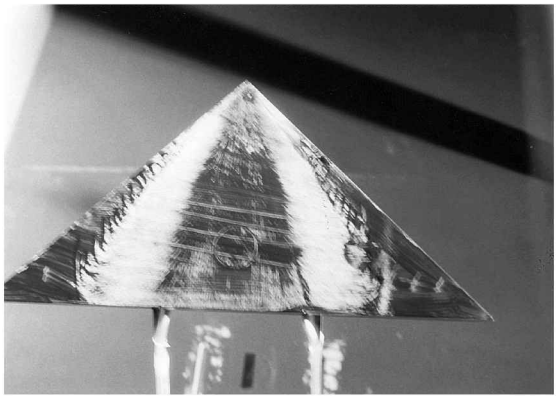

Fig. 3 Imprint of surface limiting streamlines, $\alpha = 20$ deg.

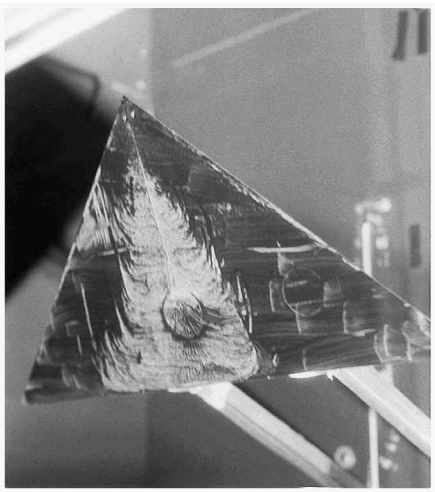

Fig. 4 Imprint of surface limiting streamlines, $\alpha = 40$ deg.

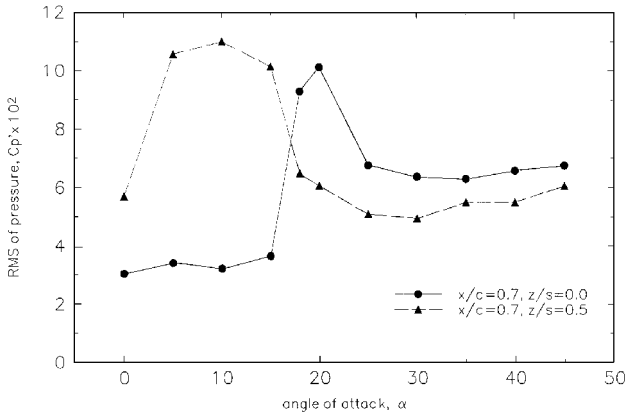

Fig. 5 Pressure fluctuations (rms).

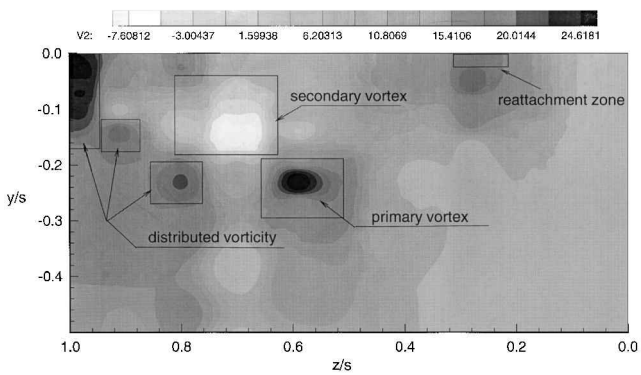

Fig. 6 Isocontour distribution of mean vorticity in the longitudinal direction: mean vorticity $\bar{\Omega}_x s/U_0$; $\alpha = 15$ deg, $X/c = 0.85$, $Re = 5.86 \times 10^4$.

pressure fluctuations decreases, most probably because the point of reattachment moves toward the plane of symmetry. The physics of the reattachment and secondary separation, as well as the formation of the secondary vortex, will be further addressed later in relation to the results of vorticity and wall vorticity flux.

The flow visualization studies of the delta wing experiment indicated a remarkable symmetry of the large primary vortical structures about the XoY plane and, therefore, hot-wire measurements were carried out in the positive z quadrant only. The measurements shown here have been obtained at a nondimensional chord location $X/c = 0.85$ when the angle of attack was 15 deg.

Data were obtained at about 100 different locations on the positive $z/$ negative y quadrant of the zoy plane of the flowfield. Spline routines were used to interpolate the data for isocontour plots. Thus, the number of data points within the original grid has been increased through interpolation. Tests were carried out to verify that this interpolation did not produce artifacts and unrealistic data by varying the number of interpolated data.

Figure 6 shows the isocontours of the mean axial vorticity projected onto a crossplane. The spanwise and normal distances are normalized by the local semi span s and vorticity by U_0/s. Strong streamwise vortical structures generated inside the shear layer as it wraps around the wing can be identified by the pockets of high positive mean axial vorticity. Peak values of normalized positive vorticity of the order of 25 have been measured inside the shear layer. That these secondary vortical structures are detected in this time-averaged distribution of vorticity indicates that they have a rather well-defined spatial pattern. The traditional secondary vortices carrying vorticity of opposite sign, known for some time to exist near the wall, can also be identified in Fig. 6 at about $z/s = 0.7$ and $y/s = \pm 0.12$. For visual aid only, the locations of high positive or negative mean vorticity peaks have been identified by black perimeter boxes. The reattachment zone is also designated similarly. For the purpose of reference, these visual aid signs are retained in all of the isocontour plots of various quantities to be shown here.

The isovelocity contours of the axial component, normalized by the incoming freestream velocity U_0, are plotted in Fig. 7. An important feature of the delta wing velocity field, which is rather difficult for prediction methods to reproduce, is the large axial velocity excess up to $1.3U_0$ observed in the region of the flow that coincides with the location of maximum mean axial vorticity. If it is assumed that the axial vorticity peaks near the center of the vortex, where pressure is lowest, then it can be argued that the flow accelerates over the apex and the axial velocity increases over its freestream value, reaching a maximum at the center of the vortex. These indicators allowed the estimation of the location of the core of the vortex to be at approximately $z/s \approx 0.55$ and $y/s \approx 0.22$, as observed in the plots of mean vorticity and mean velocity components shown in Figs. 6 and 7, respectively.

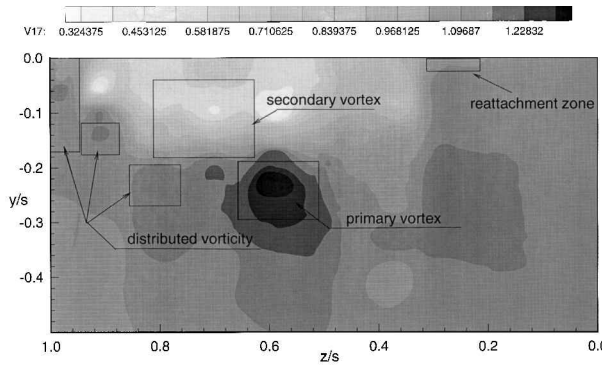

Fig. 7 Isocontour distribution of mean velocity in the longitudinal direction: mean velocity $\bar{U}/U_0$; $\alpha = 15$ deg, $X/c = 0.85$, $Re = 5.86 \times 10^4$.

In addition to the core of the primary vortex, which is characterized by a substantial velocity excess, the peaks in the distributed vorticity of the feeding shear layer are also associated with mean velocities in excess of the freestream velocity by about 10%.

It appears that there are three different regions inside the present flow that possess distinct characteristics. Besides the feeding shear layer with the distributed vorticity leading to the formation of the primary vortex, there is the wake region of the wing and the reattachment region of the wall impinging shear layer where strong shear and the adverse pressure gradient can cause bursting of the wall layer.

The most important feature of the wake region is the mean velocity defect. The results of Fig. 7 indicate a large flow region with mean velocity $0.3U_0$ in the area close to the wall and a region of high mean shear between the shear layer and the wake. The secondary vortex, which carries negative vorticity, is associated with a large velocity defect. Thus, the secondary vortex is characterized by a wakelike mean velocity profile, whereas the primary vortex is associated with a jetlike mean velocity profile. Another noticeable difference between the secondary and primary vortices is their strength. The magnitude of vorticity in the secondary vortex is only $\frac{1}{3}$ of that of the primary vortex.

Typically, although not very satisfactory, the core is defined as the region between the location where the azimuthal velocity V_θ is zero (center of the vortex) and the location where V_θ is maximum. A more meaningful and more suitable to the present case choice would be to define the core as the region of significant vorticity. According to this definition, the core size of the primary vortex appears to be $0.08s \times 0.04s$, whereas the core size of the secondary vortex is about $0.08s \times 0.08s$.

The circulation Γ of the primary vortex, which expresses its strength, was obtained by integrating the vorticity distribution over an area defined by a curve surrounding the vortex. It was found that Γ had a value of $0.08sU_0$ at the core perimeter of the vortex, whereas at a distance of $0.2s$ from the center Γ reached a value of $0.4sU_0$.

Most of the previous vorticity measurements were restricted to one-dimensional mean values. Although particle image velocimetry can yield multipoint velocity measurements on one plane, it cannot, at the present time, provide highly resolved three-dimensional and time-dependent information. In the present work, substantial mean vorticity was found in the normal and spanwise directions, indicating that the mean vorticity vector is tilted.

The distribution of the other two mean vorticity components Ω_y and Ω_z is shown in Figs. 8 and 9, respectively. In a flow with a plane

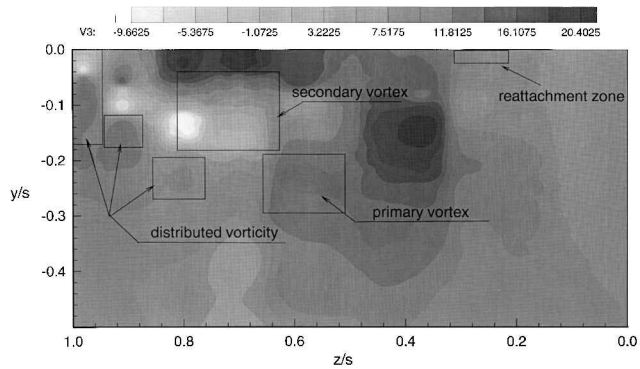

Fig. 8 Isocontour distribution of mean vorticity in the normal direction: mean vorticity $\bar{\Omega}_y s/U_0$; $\alpha = 15$ deg, $X/c = 0.85$, $Re = 5.86 \times 10^4$.

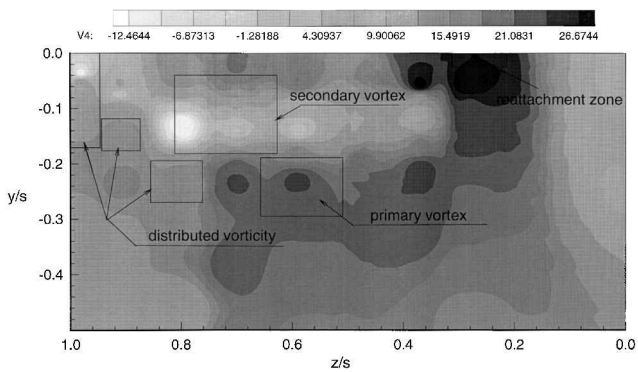

Fig. 9 Isocontour distribution of mean vorticity in the spanwise direction: mean vorticity $\bar{\Omega}_z s/U_0$; $\alpha = 15$ deg, $X/c = 0.85$, $Re = 5.86 \times 10^4$.

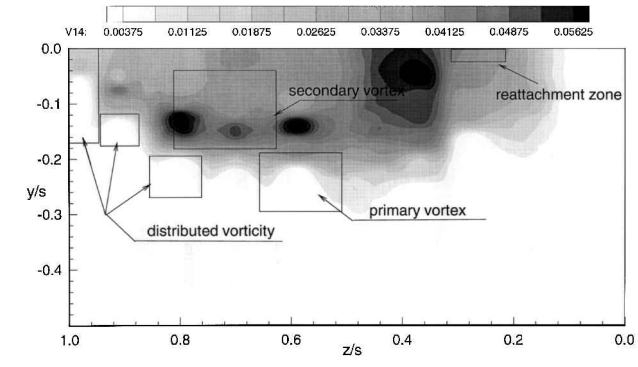

Fig. 10 Isocontour distribution of turbulent kinetic energy $\frac{1}{2}\overline{q^2}/U_0^2$; $\alpha = 15$ deg, $X/c = 0.85$, $Re = 5.86 \times 10^4$.

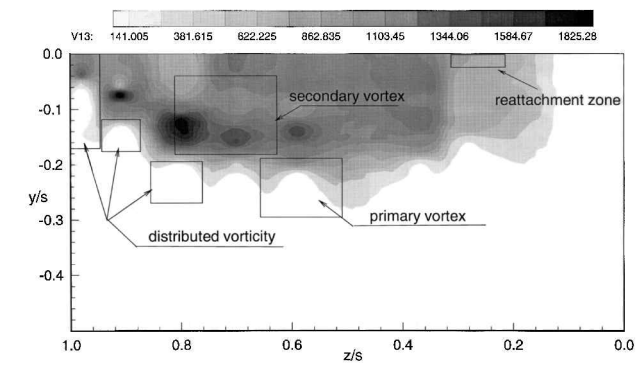

Fig. 11 Isocontour distribution of enstrophy $\frac{1}{2}(\overline{\omega_x^2} + \overline{\omega_y^2} + \overline{\omega_z^2})s^2/U_0^2$; $\alpha = 15$ deg, $X/c = 0.85$, $Re = 5.86 \times 10^4$.

of symmetry, such as the present one, Ω_x and Ω_y are expected to have an antisymmetric distribution, whereas Ω_z is expected to have a symmetric distribution about the plane of symmetry $z/s = 0$. In the first case the values of both quantities should cross zero at the plane of symmetry. The present measurements show very small values of Ω_y and Ω_x at $z/s = 0$, which are indicating that the flow is indeed symmetric. The measured values of Ω_y are rather low inside the separated shear layer region and the primary vortex, which suggests a 20-deg orientation of the vortex lines with respect the horizontal plane xoz. The Ω_z component is also small close to the leading edge and inside the shear layer, but it grows substantially away from the leading edge and reaches a nondimensional value of 21 in the region of the primary vortex and farther toward the reattachment area. The vortex line orientation with respect to the oz axis is 55 deg in the area of the primary vortex and 68 deg in the shear layer of distributed vorticity. The streamline orientation is about 110 deg in the same regions.

The maximum level of mean nondimensional vorticity in the longitudinal direction present in the flow is about 25. Measurements of mean longitudinal vorticity in a delta wing configuration with swept-back angle $\Lambda = 60$ deg, reported in the work of Agrawal et al.,[35] show a maximum value of about 17 for a vortex before burst and a value of 0.6 for a vortex after burst. The measurements of Lowson et al.[16,32] also indicate a maximum value of mean vorticity of 12 for a delta wing with $\Lambda = 85$ deg and $\alpha = 12.5$ deg. Direct quantitative comparison of these data with the present results is not possible because of the different delta wing geometries and Reynolds numbers used in the three experiments. However, some qualitative comparison can be attempted. It appears that all measurements of mean vorticity are within the same order of magnitude. It is also known that mean vorticity decreases with increasing swept-back angle Λ. Therefore, it is not a surprise that the value of mean vorticity measured in the present experiment is higher than those measured in the other two experiments. Comparison of the present data with those of Agrawal et al.[35] for the case of a vortex after burst also suggests that no bursting occurred in the present experiments.

Figure 10 shows the isocontour distribution of turbulent kinetic energy $\frac{1}{2}q^2$ normalized by U_0^2. The distribution of the individual normal stresses of the complete Reynolds stress tensor is very similar to the distribution of turbulent kinetic energy. The most striking feature of the distribution of turbulent kinetic energy is its extremely low values measured inside the feeding shear layer. Turbulence is mainly confined in the wake region; in the region of high shear, which is located between the wake and the shear layer; and in the reattachment zone. Therefore, it appears plausible to consider the entire high-speed side of the feeding shear layers turbulence free and, in particular, the core of the primary vortex as nonturbulent.

There are several peaks of $\frac{1}{2}q^2$ in the high mean shear region of the flow, which indicate substantial turbulent activities. This region is characterized by large mean velocity gradients $\partial\overline{U}/\partial y$ and $\partial\overline{U}/\partial z$, whereas the peaks of $\frac{1}{2}q^2$ coincide with the location where these gradients are at maximum. Three of the four peaks are associated with the secondary vortex, which appears to be highly turbulent, whereas the fourth peak is located next to the reattachment zone. The area between the secondary vortex and the primary vortex or distributed vorticity, i.e., the low-speed side of the shear layer, is the high shear region where the mean velocity U increases from $0.3U_0$ to $1.3U_0$, i.e., a $1.0U_0$ velocity change within a rather small distance.

The level of vorticity fluctuations in the present flow can be seen in Fig. 11, where isocontours of nondimensionalized fluctuating enstrophy are plotted. The extent of the region with substantial enstrophy distribution is remarkably similar to that of $\frac{1}{2}q^2$. The high-speed side of the shear layer and, in particular, the core of the primary vortex are characterized by an extremely low level of fluctuating vorticity suggesting a rather stationary pattern of the vortex and of the region with distributed vorticity. On the contrary, the low-speed side of the shear layer, where the mean shear is extremely high, seems to be associated with a highly fluctuating vorticity field. The maximum value of enstrophy fluctuations appears to be about twice the value of the square of the mean vorticity Ω_x measured at the core of the primary vortex and takes place at the location of maximum mean vorticity gradients. Consideration of the transport equation for $\omega_i\omega_i$ suggests that the gradient production term $-\overline{u_j\omega_i}\partial\overline{\Omega_i}/\partial x_j$ is a source term that indicates the exchanges of vorticity between $\omega_i\omega_i$ and $\Omega_i\Omega_i$ (Ref. 30). This process is similar to that described by the

turbulent kinetic energy production term $-\overline{u_i u_j} S_{ij}$, which shows the exchange of energy between $U_i U_i$ and $u_i u_i$. The present data indicate that the gradient production term $-\overline{u_j \omega_i} \partial \overline{\Omega_i} / \partial x_j$ has the most dominant contribution in the balance of fluctuating enstrophy.

The physics related with this highly fluctuating vortical field is not yet understood. A spatial wandering of the secondary vortex in the yoz plane may cause substantial vorticity fluctuations. This explanation seems to be quite plausible bearing in mind that the vortex originated at the wall and that its mean position found away from the wall. However, this phenomenon cannot account entirely for the high levels of vorticity fluctuations, particularly for the positive ones, which are opposite in sign to that of mean vorticity. The mean vorticity Ω_x of the secondary vortex, for instance, is about -8 (see Fig. 6), whereas the rms of the ω_x fluctuations about the mean value is of the order of 35 (not shown here). Thus, a substantial amount of fluctuation appears to be of opposite sign to that of mean Ω_x. Spatial wandering of the secondary vortex cannot explain the presence of opposite sign vorticity.

A second mechanism, based on the well-known structures of rolls and ribs found in two-dimensional shear layers separated from sharp edges normal to the flow, may provide some explanation of the physics of this flow region. Rolls are the nominally spanwise vortical structures that are connected by counter-rotating longitudinal vortices, the ribs. As the sweep angle of this sharp edge increases, it is very possible that this basic structure still exists but the rolls and the ribs are swept backwards and stretched in the longitudinal direction. It is obvious that the ribs and rolls have a substantial component of vorticity in the longitudinal direction. The rolls contribute to the primary vortex and the distributed vorticity of the shear layer, whereas the counter-rotating vorticity of the ribs is part of the vorticity found in the secondary vortex. This explanation basically implies that a helical mode of instability is present in the swept-back shear layer, a hypothesis that is very possibly true but not yet proven theoretically to exist in this flow.

A third mechanism that has to be considered is the existence of a Taylor–Görtler type of instability, which may produce vortices of alternative sign. These counter-rotating vortices may cause the large rms values measured in this region of the flow. This instability is a result of destabilizing effects of centrifugal forces associated with streamline curvature. The curvature Richardson number $Ri = -2U/R/[\partial U/\partial y + U/R]$, where R the radius of curvature, is the parameter that defines the destabilizing or stabilizing effect of streamline curvature. A typical mean velocity profile (such as that shown schematically in Fig. 12) is not monotonic and contains two inflectional points. A spiral streamline is shown around the vortex. The sketch indicates that streamline curvature can be convex or concave. In the outer part of the vortex, streamline curvature has a destabilizing effect and a stabilizing effect in the inside region between the vortex and the leading edge where the feeding shear layer is located. Thus, Taylor–Görtler vortices most probably cannot exist in the inside region. Even in the region across the vortex, where streamline curvature could cause instability, the Richardson number reaches very low values, indicating that centrifugal forces are not large enough to initiate the instability process. This also explains the lack of vorticity fluctuations in the outer region of the vortex. Thus, the most likely mechanism appears to be that of a helical mode of instability.

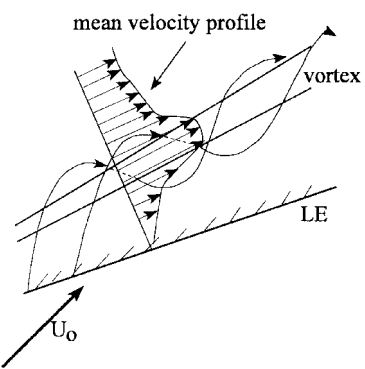

Fig. 12 Schematic of streamline curvature effects.

It is rather difficult to define the mean position of reattachment of a spiraling three-dimensional shear layer from mean velocity measurements, particularly in a vortex dominated flow, which contains no stagnating streamlines. In the present context, reattachment is defined as the region of the flowfield where mean V and mean Ω_y vanish. This definition, although not entirely satisfactory, is supported by the measurements, as well as by the flow visualization results, particularly the surface imprints of the limiting streamlines. As the separated shear layer approaches the wing surface, considerable reorientation of the vorticity field takes place to satisfy the boundary condition $\Omega_y = 0$ at the solid surface. It is particularly interesting to see in Fig. 8 the gradual decrease of mean Ω_y in the area below the reattachment zone, which is also associated with a reduction in mean V (not shown here). The presence of a strongly negative gradient $\partial V/\partial y$ in this region compresses the vortex lines and, thus, it reduces Ω_y. Note that the requirement for $\Omega_y = 0$ at the surface at all times is a result of the no-slip condition at the wall, which holds for the entire surface of the delta wing, not only for the reattachment zone. The particular feature of the present reattachment zone is that mean Ω_y approaches zero at several locations away from the solid wall. At the same time, the component of vorticity in the spanwise direction increases considerably, indicating a substantial reorientation of the mean vorticity vector in that area. This is shown in Fig. 9, where the distribution of mean Ω_z is plotted. Values of nondimensional $\Omega_z s/U_0$ up to 25 can be observed in the reattachment zone. However, these high values of Ω_z cannot be entirely attributed to reorientation of shear layer vorticity. New vorticity is generated at the wall by the high-speed fluid of the reattaching shear layer moving in the vicinity of the wall because of the no-slip condition at the wall. As a result of this interaction between the wall and the reattaching spiral shear layer, which is characterized by high shear, the flow produces a large amount of turbulent kinetic energy, as shown in Fig. 8. Thus, the reattaching shear layer becomes turbulent, followed by the generation of new vorticity Ω_z.

According to the flow visualization results, secondary separation of the wall layer has taken place at about $z/s = 0.66$. This area is located above the secondary vortex, and the measurements indicate some flow features that provide evidence of sudden bursting of the wall layer. The mean flow components suggest an outward flow direction, i.e., away from the wall while mean Ω_y and Ω_z reach high values. Large values of vorticity and velocity fluctuations are also present in this region, which is indicative of the highly unsteady nature of the flow.

Wall Vorticity Flux

The quantity that describes the process of vorticity production at a solid boundary is the vorticity gradient normal to the wall $-[\partial\omega/\partial y]_{\text{wall}}$, which is called vorticity flux density, a term first introduced by Lighthill,[37] who defined it for two-dimensional flows by analogy to Fourier's heat conduction. The term vorticity flux describes the rate of vorticity production at the wall, which then enters the flow. In that sense it is more important to know the amount of vorticity entering the flow than vorticity at the wall. However, vorticity dynamics inside the flow are best described by using vorticity as a variable. According to the theory of Wu and Wu,[38] vorticity flux can be directly linked to the aerodynamic forces of lift and drag acting on a body.

The momentum equation evaluated at the wall, where the velocity vector is identically zero because of no-slip conditions, yields

$$\frac{\partial p}{\partial x} = -\mu \frac{\partial \omega_z}{\partial y} \tag{2}$$

and

$$\frac{\partial p}{\partial z} = \mu \frac{\partial \omega_x}{\partial y} \tag{3}$$

At the wall, there is no stretching of vortex lines and the term $S_{ik}\Omega_k$ in the transport equation of vorticity (1) vanishes so that the rate of change of vorticity is entirely produced by the diffusion term

$$\left[\frac{\mathrm{D}\Omega_i}{\mathrm{D}t}\right]_w = \left[\nu \frac{\partial^2 \Omega_i}{\partial x_k \partial x_k}\right]_w$$

The preceding equations indicate that the wall pressure gradient is generating a flux of vorticity into the fluid and show that there is a strong coupling between pressure and vorticity. This relationship is not apparent in the vorticity transport equation because the latter does not include any pressure terms as shown in Eq. (1). If these pressure gradients can be measured instantaneously, then the vorticity flux away from the wall can be computed as a time-dependent function.

Four miniature pressure transducers supplied by Kulite semiconductor were used to measure the required pressure gradients in two directions. Details of the techniques used and a discussion on the results obtained in a two-dimensional boundary layer can be found in the recent work by Andreopoulos and Agui.[4] In the present case, the module with the four transducers was inserted at two different positions on the delta wing, one on the line of symmetry at $z/s = 0.0$ and the second at $z/s = 0.5$.

In the present context, the coordinate system is aligned with the surface of the wing. Thus, the vorticity flux tangential to the wall

$$\sigma_w = -\nu\left[\frac{\partial \omega_x}{\partial y}\right]_w i - \nu\left[\frac{\partial \omega_z}{\partial y}\right]_w k$$

can be directly estimated from the two measurable pressure gradients. The third component in the normal to the wall direction, $\partial \omega_y/\partial y$, could not be measured.

One remarkable property of vorticity and vorticity flux is that fluctuations are considerably larger than the corresponding means. The measurements of vorticity shown earlier indicated that mean Ω_x is about five times less than the rms of the fluctuations ω_x. Measurements of mean pressure gradients also were found to be substantially lower than the fluctuations. Consequently, the effect of mean vorticity flux can be considered as marginal.

Because vorticity is generated at the wall where strong viscous effects are present, the use of appropriate viscous scales to normalize the results is justified. If u_T is the friction velocity, then the viscous length scale is ν/u_T. The value of u_T used in the data presentation was chosen arbitrarily to be $0.05U_0$ because measurement of skin friction was not attempted. In a separated three-dimensional boundary layer such as the present flow, such measurement is extremely difficult to carry out and the resulting estimates of skin friction can be highly inaccurate. The value used here for normalization of the results suggests a skin-friction coefficient of the order of 0.005.

Figure 13 shows the normalized rms of vorticity flux fluctuations as a function of the angle of attack measured at two different spanwise locations on the delta wing. Both locations are at $x/c = 0.7$, a position that is upstream of the location $x/c = 0.85$ where the three-dimensional vorticity measurements were carried out. Thus, vorticity shed off the wall and measured by the Kulite module could be detected by the hot-wire probe, which was placed at a downstream location. The data of Fig. 13 indicate a behavior very similar to that of the pressure fluctuations shown in Fig. 5. At the centerline, $z/s = 0.0$, the level of fluctuations of both components $\partial \omega_x/\partial y$ and $\partial \omega_z/\partial y$ is rather low, in the range of 0–15-deg angle of attack. It increases substantially at $\alpha = 20$ deg and retains high values at $\alpha > 30$ deg.

The distribution of the same vorticity flux components at $z/s = 0.5$, a location off the centerline, is rather different. Large fluctuations occurred at small angles of attack, whereas the level of fluctuations at $\alpha > 15$ deg was considerably reduced.

Secondary Vorticity

The results of vorticity flux at the surface of the delta wing indicate that strong vortical activities take place in the near-wall region. The fact that there is new vorticity production at the wall provides evidence, shown experimentally for the first time, that, indeed, there is secondary vorticity generated at the surface of the delta wing. The generation of a secondary vortex has been shown theoretically to exist. However, very few of the theoretical works that dealt with the problem of induced vorticity in the region close to the wall were able to predict the process of secondary vorticity generation in a time-dependent manner with adequate spatial resolution to capture details of the generation and evolution of the vortical structure.

It is known that the vorticity of the primary vortex is basically originated and mostly generated at the leading edge of the wing. If the origin of this vorticity is to be investigated in more detail, then the vorticity flux at the leading edge should measured. The focus of the investigation, however, was the new vorticity produced by the induced action of the primary vortex and the no-slip conditions at the wall. Thus, the vorticity flux module was placed at the wall approximately in the area below the primary vortex and at the centerline of the wing. Our results indicate that this vorticity generation is a function of the angle of attack and the location at the wall. At small angles α, for instance, there is substantial production of vorticity at $z/s = 0.5$, a location that is very close to the reattachment region of the induced flow where fluid impinges on the wall; it is subsequently deflected to the sides and, because of the wall friction and strong shearing, new vorticity is generated at the wall. As the angle of attack increases, this region of reattachment moves from regions closer to the leading edge toward the centerline.

It is also interesting to observe that this process of new vorticity production is not laminar. The large fluctuations of the signal also suggest that the process is very intermittent and that positive as well as negative vorticity can be generated. Thus, the induced secondary vorticity contains not only vorticity opposite in sign to the vorticity of the inducing primary vortex but also vorticity of the same sign as the primary vortex. It is possible for the induced vorticity, in the form of a vortex, to induce vorticity of opposite sign for a second time, which is the same as the sign of vorticity of the original primary vortex. The experimental evidence clearly shows that vorticity at the wall changes sign very often. Thus, in the present case of a turbulent near-wall region, there is a continuous production of vorticity with positive or negative sign, which suggests that the wall acts as a source or sink of vorticity.

The highly fluctuating nature of the wall vorticity flux vector is also demonstrated in the plots of Fig. 14, where the probability density function (PDF) of the orientation angle θ with respect the positive spanwise direction is shown for two typical values of angle of attack α at two locations, $z/s = 0.0$ and 0.5, where measurements were carried out. This angle θ can vary between 180 and -180 deg and is positive in the clockwise direction. Statistical analysis has shown rms values of the order of 98 deg, which is indicative of a highly fluctuating vector σ_w.

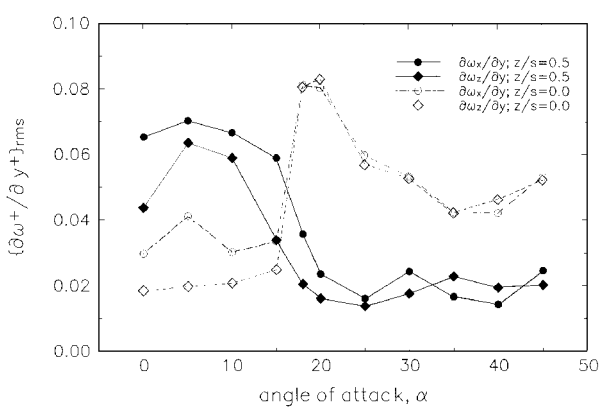

Fig. 13 Fluctuations of wall vorticity flux at *x/c* = 0.7.

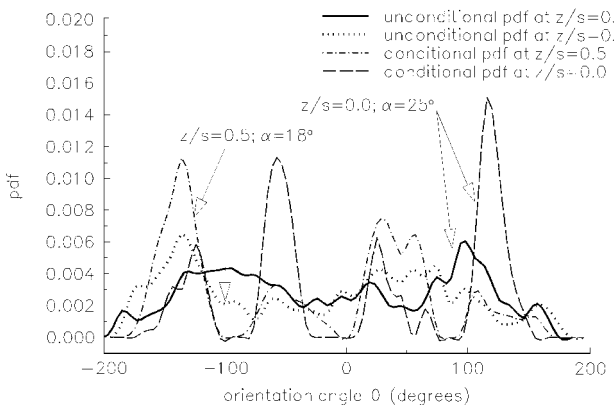

Fig. 14 PDF of orientation angle at *x/c* = 0.7.

The orientation of σ_w during violent events, which are associated with large excursions in amplitude, is of particular interest. To investigate the behavior of these events, conditional analysis has been applied to the vorticity flux signals. The detection scheme is based on threshold level set at one rms value of the fluctuations. Interrogation of the sign of each signal determined the algebraic value of θ. The conditional PDFs of θ are also shown in Fig. 14.

Symmetry requirements of the unconditioned PDF at $z/s = 0.0$ suggest that this distribution should be symmetric about the longitudinal axis, which corresponds to $\theta = \pm 90$ deg. The distribution for $z/s = 0.0$ shows peaks at $\theta = +90$ and -90 deg and a reasonable symmetry about these two directions. At $z/s = 0.5$, a position off the plane of symmetry, no symmetrical distribution is expected. Indeed, the unconditioned PDFs show a sharp peak at $\theta = -135$ deg and a relatively flat peak at a about 150 deg.

It is very remarkable to observe the drastic changes in the most probable values of all PDFs when the data are conditioned. The application of a small threshold to the data changes significantly the distributions by filtering out all small-amplitude contributions and reveals some organization in the distribution of θ, which suggests that relatively large-amplitude events are oriented in preferential directions of rather narrow band. At $z/s = 0.0$, the symmetry requirements no longer apply to the conditioned data and new peaks appear at 115, 55, 25, -55, and -130 deg. The peaks at -55 and 115 deg are the most dominant.

At $z/s = 0.5$, local peaks at about 110, 55, 20, -55, and -135 deg can be also observed. Both cases of PDF distributions clearly suggest that any new vortical structure generated at the wall during strong events carries vorticity that is not aligned in the longitudinal or spanwise only direction. It is clearly tilted in some preferential direction.

Discussion and Conclusions

An attempt has been made to measure the three-dimensional, time-dependent vorticity field in the flow over a delta wing at 15-deg angle of attack. A large amount of three-dimensional vorticity and velocity data has been acquired.

The results of the study confirm the existence of a primary vortex where mean vorticity is at a maximum and where the mean velocity excess is about $1.3U_0$. In addition to the large velocity excess, the core has been found to be turbulence free. As a result of the no-slip condition at the surface of the wing, a secondary vortex of opposite sign to that of the primary vortex is formed. This vortex leaves the wall region and moves toward the low-pressure region of the primary vortex. New experimental techniques have been used to measured the secondary vorticity flux at the wall of the delta wing. For the first time, experimental evidence has been produced to show that vorticity of alternating sign is generated at the surface of the wing. Large fluctuations of the orientation of the vorticity flux vector were found to take place. This suggests that the flow structure in the near-wall region is very complicated. However, the data show that there are some preferential orientations of the vorticity flux vector, which ought to be investigated further. It has been shown experimentally in two-dimensional boundary layers that there is a propensity of alignment between vorticity and eigenvectors of the strain-rate tensor S_{ij} (Ref. 28). It is very likely that the most probable orientation found in the present analysis is closely related to the eigenvectors of the strain-rate tensor at the wall.

There is considerable distributed vorticity in the shear layer, which leads to the formation of several discrete vortices that remain stationary in space. Although there is continuous distribution of vorticity around the primary vortex, no discrete secondary vortices located around the primary vortex were found in the present case, a behavior that is in contrast to the case of the highly swept-back delta wings of Payne et al.[14] and Lowson et al.[32] The present measurements indicated the existence of discrete vortices in the shear layer region only. It is suggested here that these discrete vortices are typical shear layer rollups, which are due to Helmholz–Kelvin-type instabilities, most probably of the helical mode. The candidate structure is based on the typical structure of a two-dimensional shear layer, as has been proposed by Bernal.[33] The basic structure consists of two topologically unconnected vortex pairs, which at the locations of the rollups, have sections with vortex lines parallel to each other and of the same sign vorticity. Thus, locally, vorticity appears to be stronger. The model also explains the direction of the measured vorticity close to the leading edge in the separated shear layer.

Most of the turbulent activities take place in the area between the separated shear layer and the delta wing. The peaks in the rms of vorticity or velocity fluctuations occur in the low-speed side of the separated shear layer and close to the edge of the core of the vortex. The core apparently is a region with rather low-turbulence intensity. The shear layer reattachment zone and the area of secondary separation are associated with high-turbulence activities.

It has been reported recently that a pair of counter-rotating structures exists below the primary vortex and close to the reattachment region, which has a size of $0.1s \times 0.1s$ and is aligned in the spanwise direction.[39] Our vorticity flux measurements at the wall of the delta wing also indicate the existence of structures that may be aligned in directions other than the longitudinal one. In addition, the vorticity data obtained near the reattachment zone show large values of all mean vorticity components and large values of vorticity fluctuations. Presumably, these large mean vorticity values indicate the existence of a vortex that subsequently induces the generation of new vorticity at the wall as a result of the no-slip conditions at the wall. Because nature usually has vortices in pairs, this new vortex immediately induces a new vortex of opposite sign so that a pair of counter-rotating vortices appear. The generation of new vorticity through the no-slip conditions at the wall appears to be the predominant mechanism for the appearance of new vortices rather than the Taylor–Görtler instability mechanism that requires a large value of Richardson number with a destabilizing effect of streamline curvature. Thus, the flow after reattachment appears to be considerably more complicated than is traditionally depicted by computational fluid dynamics algorithms.

Acknowledgments

The financial support provided by National Science Foundation is gratefully acknowledged. The authors would like to thank J. Agui for his comments on this work.

References

[1] Squire, L. C., "An Experimental Investigation of the Characteristics of Some Plane and Cambered 650 Delta Wings at Mach Numbers from 0.7 to 2," Aeronautical Research Council, Repts. and Memoranda No. 3305, 1961.

[2] Polhamus, E. C., "Sharp-Edge Delta Wings Based on the Leading Edge Suction Analogy," NASA TN-D-3767, 1966.

[3] Doligalski, T. L., Smith, C. R., and Walker, J. D., "Vortex Interactions with Walls," *Annual Review of Fluid Mechanics*, Vol. 26, 1994, pp. 573–616.

[4] Andreopoulos, J., and Agui, J., "Wall Vorticity Flux Dynamics in a Two-dimensional Boundary Layer," *Journal of Fluid Mechanics*, Vol. 309, 1996, pp. 45–84.

[5] Hall, M. G., "Vortex Breakdown," *Annual Review of Fluid Mechanics*, Vol. 4, 1972, pp. 195–218.

[6] Leibovich, S., "Vortex Stability and Breakdown," *AIAA Journal*, Vol. 22, No. 9, 1984, pp. 1192–1206.

[7] Towfighi, J., and Rockwell, D., "Transient Structure of Vortex Breakdown on a Delta Wing via Particle Image Velocimetry," *AIAA Journal*, Vol. 31, No. 6, 1993, pp. 1160–1162.

[8] Rockwell, D., "Three Dimensional Flow Structure on Delta Wings at High Angles of Attack," AIAA Paper 93-0550, Jan. 1993.

[9] Visbal, M. R., "Computational and Physical Aspects of Vortex Breakdown on Delta Wings," AIAA Paper 95-0585, Jan. 1995.

[10] Ayoub, A., and McLachlan, B. G., "Slender Delta Wing at High Angles of Attack—A Flow Visualization Study," AIAA Paper 87-1230, 1987.

[11] Gad-el-Hak, M., and Blackwelder, R. F., "Control of the Discrete Vortices from a Delta Wing," *AIAA Journal*, Vol. 25, No. 8, 1987, pp. 1042–1049.

[12] Gad-el-Hak, M., and Blackwelder, R. F., "The Discrete Vortices from Delta Wing," *AIAA Journal*, Vol. 23, No. 5, 1985, pp. 961, 962.

[13] Lowson, M. V., "Visualization Measurements of Vortex Flows," *Journal of Aircraft*, Vol. 28, No. 5, 1991, pp. 320–327.

[14] Payne, F. M., Ng, T. T., Nelson, R. C., and Schiff, L. B., "Visualization and Wake Surveys of Vortical Flow over a Delta Wing," *AIAA Journal*, Vol. 26, No. 2, 1988, pp. 137–143.

[15] Sforza, P. M., Stasi, W., Pazizienza, J., and Smorto, M., "Flow Measurements in Leading Edge Vortices," *AIAA Journal*, Vol. 16, No. 3, 1978, pp. 218–224.

[16] Lowson, M. V., Riley, A. J., and Swales, C., "Flow Structure over Delta Wings," AIAA Paper 95-0586, Jan. 1995.

[17] Visser, K. D., and Nelson, R. C., "Measurements of Circulation and Vorticity in the Leading Edge Vortex over a Delta Wing," *AIAA Journal*, Vol. 31, No. 1, 1993, pp. 104–111.

[18] Ekaterinaris, J., and Schiff, L. B., "Numerical Prediction of Vortical Flow over Slender Delta Wings," *Journal of Aircraft*, Vol. 30, No. 6, 1993, pp. 935–942.

[19] Washburn, A. E., and Visser, K. D., "Evolution of Vortical Structures in the Shear Layer of Delta Wings," AIAA Paper 94-2317, 1994.

[20] Andreopoulos, J., "Improvement of the Performance of Triple Hot-Wire probes," *Review of Scientific Instruments*, Vol. 54, 1983, pp. 733–740.

[21] Andreopoulos, J., "Statistical Errors Analysis Associated with Probe Geometry and Turbulence Intensity in Triple Hot-Wire Anemometry," *Journal of Physics E: Scientific Instruments*, Vol. 16, 1983, pp. 1264–1271.

[22] Maciejewski, P. K., and Moffat, R. J., "Interpreting Orthogonal Triple-Wire Data From Very High Turbulence Flows," *Journal of Fluids Engineering*, Vol. 116, 1994, pp. 463–468.

[23] Honkan, A., "An Experimental Study of the Vortical Structure of Turbulent Flows," Ph.D. Thesis, Mechanical Engineering Dept., City College of the City Univ., New York, NY, 1994.

[24] Honkan, A., and Andreopoulos, J., "Direct Calibration Mapping and Data Analysis in Triple Hot-Wire Anemometry," *Thermal Anemometry*, edited by D. Stock, S. A. Serif, and A. J. Smits, FED-Vol. 167, American Society of Mechanical Engineers, New York, 1993, pp. 67–78.

[25] Andreopoulos, J., and Honkan, A., "Conditional Statistics of Time-Resolved Vorticity and Vorticity Flux in the Wall Region of Turbulent Boundary Layer Flow," AIAA Paper 94-2303, June 1994.

[26] Balint, J., Wallace, J. M., and Vukoslavcevic, P., "The Velocity and Vorticity Vector Fields of a Turbulent Boundary Layer. Part 2 Statistical Properties," *Journal of Fluid Mechanics*, Vol. 228, 1991, pp. 53–86.

[27] Spalart, P. R., "Direct Numerical Simulation of a Turbulent Layer up to Re = 1410," *Journal of Fluid Mechanics*, Vol. 187, 1988, pp. 61–86.

[28] Honkan, A., and Andreopoulos, J., "Vorticity, Strain-Rate and Dissipation Characteristics in the Near Wall of Turbulent Boundary Layers," *Journal of Fluid Mechanics* (to be published).

[29] Thomas, J. L., Krist, S. T., and Anderson, W. K., "Navier–Stokes Computations of Vortical Flows over Low Aspect Ratio Wings," *AIAA Journal*, Vol. 28, No. 2, 1990, pp. 205–212.

[30] Tennekes, H., and Lumley, J. L., *A First Course in Turbulence*, MIT Press, Cambridge, MA, 1972.

[31] Wallace, J. M., and Foss, J. F., "The Measurement of Vorticity in Turbulent Flows," *Annual Review of Fluid Mechanics*, Vol. 27, 1995, pp. 469–514.

[32] Lowson, M. V., Riley, A. J., and Rwales, C., "Flow Structure over Delta Wings," AIAA Paper 95-0586, Jan. 1995.

[33] Bernal, L. P., "The Coherent Structure of Turbulent Mixing Layers. II: Secondary Streamwise Vortex Structure," Ph.D. Thesis, California Inst. of Technology, Pasadena, CA, 1981.

[34] Andreopoulos, Y., and Honkan, A., "Experimental Techniques for Highly Resolved Measurements of Rotation, Strain and Dissipation Rate Tensors in Turbulent Flows," *Measurement Science and Technology*, Vol. 7, No. 10, 1996, pp. 1462–1476.

[35] Agrawal, S., Barnett, R. M., and Robinson, B. A., "Numerical Investigation of Vortex Breakdown on a Delta Wing," *AIAA Journal*, Vol. 30, No. 3, 1992, pp. 584–591.

[36] Andreopoulos, Y., and Honkan, A., "The Measurement of the Velocity Gradient Tensor in Turbulent Flows: A Challenge for the Experimentalist," *4th International Symposium on Thermal Anemometry*, edited by D. Stock, S. A. Serif, J. Davidson, and A. J. Smits, FED Vol. 236, No. 4, American Society of Mechanical Engineers, New York, 1996, pp. 241–264.

[37] Lighthill, M. J., "Boundary Layer Theory," *Laminar Boundary Layers*, edited by L. Rosenhead, Oxford Univ. Press, Oxford, England, UK, 1963, p. 46.

[38] Wu, J.-Z, and Wu, J. M., "Interaction Between a Solid Surface and a Viscous Compressible Flow Field," *Journal of Fluid Mechanics*, Vol. 254, 1993, pp. 183–211.

[39] Hubner, J. P., and Komerath, N. M., "Counter-Rotating Structures over a Delta Wing," *AIAA Journal*, Vol. 34, No. 9, 1996, pp. 1958–1960.

D. Parekh
Associate Editor